35th Annual International Conference of the IEEE EMBS
Osaka, Japan, 3 - 7 July, 2013

Accurate and Continuous Non-Contact Vital Signs Monitoring Using Phased Array Antennas in a Clutter-Free Anechoic Chamber

A. Boothby, V. Das, J. Lopez, J. Tsay, T. Nguyen, R.E. Banister and D.Y.C Lie, *Sr. Member, IEEE*

***Abstract*— Continuous and accurate monitoring of human vital signs is an important part of the healthcare industry, as it is the basic means by which the clinicians can determine the instantaneous status of their patients. Doppler-based non-contact vital signs (NCVS) sensor systems can monitor the heart and respiration rates without touching the patient, but it has been observed that that the accuracy of these NCVS sensors can be diminished by reflections from background clutters in the measurement environment, and that high directivity antennas can increase the sensing accuracy. Therefore, this work explores a NCVS sensor with continuous data taken inside an anechoic chamber where the background cluttering is negligible. In addition, a high directivity custom-made beam-steerable phased array antenna system is used to improve the performance and functionality of the 2.4GHz NCVS sensor we have built. We believe this work is the 1st systematic study using Doppler-based phased array systems for NCVS sensing performed in a clutter-free anechoic chamber.**

I. Introduction

The ability to capture, record, and analyze vital signs information quickly can make a life-and-death difference in the ability for clinicians to make quick and informed decisions about patients' conditions for treatments. The most common vital signs measured in a hospital setting are: temperature, blood pressure, heart rate and respiratory rate [1]. In most cases, temperature and blood pressure are measured by single samples taken over a relatively longer period (say in every 4 to 8 hours), meaning that equipment is only needed while the measurement is being taken. However, heart rate and respiration rate information may need to be captured continuously when a patient is under observation or in critical conditions such as in surgery, in an intensive care unit (ICU) or during an emergency room (ER) visit. Historically and normally, heart and respiration rates are measured by devices which physically contact the subject in order to sense, display, and record the information. Needless to say, these devices are all either wearable sensors or physically invasive to the subject, causing unavoidable discomfort or pain to the patients if one would need to take these vital signs measurement continuously. This has led to research efforts into the use of wireless and non-contact measurement systems to measure these vital signs (heart and respiration rates). The concept of measuring physical vital signs through wireless means has existed since the 1970's [2,3]. Most research into wireless non-contact vital signs (NCVS) sensor systems incorporates the use of Doppler-radar based RF signals to measure the periodic movement of a patient [4-7]. A Doppler radar target with periodic motion and zero average velocity will generate a nonlinear phase modulation which is proportional to the position of the target [6,7]. Because both heart and respiration movements cause a time-varying periodic motion at the patient's chest, the patient can be illuminated by the Doppler radar system using appropriate and safe radiation levels, which in turn allows the system to gather information about the vital statistics of the patient. The details of the NCVS sensor system itself using a fixed non-steerable beam and with several different antennas have been described previously in [8-9]. In this paper, the performance and accuracy of the NCVS biosensor is determined by the statistical analysis of a large amount of continuous-time data it collected and compared with the heart rate data measured from a physical and independent finger pulse sensor as the reference. We believe this work is the 1st systematic study using phased array antennas for NCVS sensing performed in a clutter-free anechoic chamber, and it can shed some new lights on the understanding and improvement of current fixed-beam NCVS sensor systems.

Authors are with the Dept. of Electrical and Computer Engineering, Texas Tech University, Lubbock, TX 79409-3102, USA. T. Nguyen, R.E. Banister and D.Y.C. Lie are also with the Texas Tech University Health Sciences Center (TTUHSC), Texas Tech University, Lubbock, TX, USA (e-mail: donald.lie@ttu.edu).

II. Fixed Beam and Phased-Array NCVS Sensors

A. 2.4GHz Fixed-Beam NCVS Sensor System

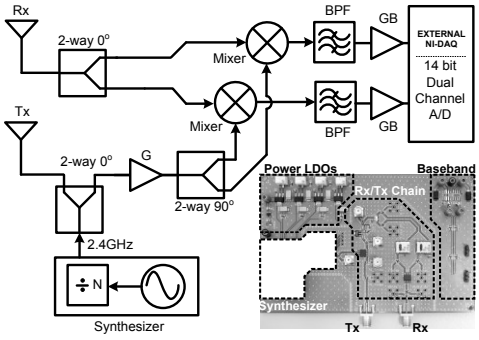

Fig. 1 (a) System block diagram for our fixed beam portable Doppler based NCVS monitoring system; (b) an image of the vital signs sensor in Fig. 1(a) implemented on a PCB, with functional regions outlined (an external NI-DAQ shown in Fig. 1(a) is not included in the PCB image)

First, the system block-level diagram of our 2.4GHz fixed beam NCVS sensor is shown in Fig. 1(a) with the corresponding board level image in Fig. 1(b). The receive (Rx) section consists of a 2-way 0° balun that splits the received signal and provides the RF input into I/Q mixers. A circulator was not used since it is bulky and may cause self-mixing. The transmit (Tx) CW signal is generated by a frequency synthesizer with an external oscillator reference and exhibit excellent phase noise. The mixer LO port and the

transmitted signal utilize the same source to take advantage of range correlation. The synthesizer output is split by a 2-way 0° balun to feed the Tx antenna, and a 2-way 90° degree splitter to create the 0/90° LO signal for the I/Q mixers. After the I/Q mixers stage, the signal is further conditioned with Sallen-Key 2nd order low-pass and high-pass filters with cutoff frequencies at 10 and 0.1 Hz, respectively, using non-inverting op-amps with a voltage gain of 60 dB. This allows us to eliminate a bulky LNA stage typically used in some other systems [10,11]. The baseband signal is digitized at a sampling rate of 200 Hz with a National Instruments (NI) USB-6009 Multifunction Data Acquisition Unit (DAQ), which uses a 14-bit ADC with a maximum sampling rate of 48 kS/s, adequate for vital signs detection resolution after baseband filtering.

B. Phased Array Antenna for NCVS Sensor in Anechoic Chamber

The phased arrays can not only provide increased directivity, but can also control the direction of the main radiation lobe within certain limits, which are usually determined by the radiation performance, i.e., directivity and Half-Power Beam-Width (HPBW) of the individual antenna making up the array. The most common type of testing environment for smaller scale antennas such as those developed in this work is the indoor free space range anechoic chamber, and the phased array sensors are tested in the anechoic chamber we built. There are multiple ways of achieving phase control over the array, including active and passive phase shifters. In the case of this work, basic passive phase control is developed from the employment of simple 50Ω delay lines with carefully designed lengths. The phase inputs to the antenna elements in the array are controlled by tuned phase delay modules (PDM's), which are connected to the outputs of a phase-balanced power splitter. The outputs of the PDM's are connected to the antennas with equal length SMA cables, as shown in Fig. 2. This ensures that the only phase offset between the channels is introduced by the PDM's.

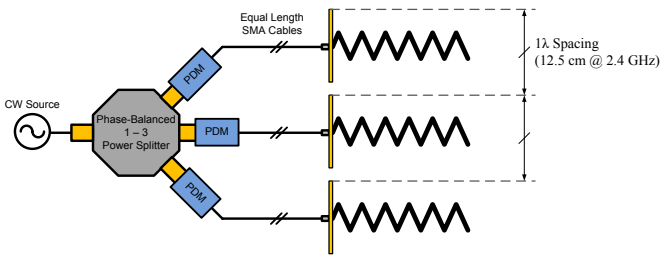

Fig. 2 Functional diagram of the Phase Delay Modules (PDM) used to control the phase input to individual helical antenna elements in the array.

The following pages show the Matlab simulations of an ideal array of 8-turn helical antennas. We have also added some pattern analysis code that determined the HPBW and steering angles of the pattern results. The Matlab code is based on the basic MxN-element array factor equations for a planar array as outlined in Balanis [12], and the axial mode helical antenna array factor equations from Kraus [13]. This approximation uses a Hansen-Wooyard endfire array factor for the helical antenna itself is from [13]:

$$AF_h = \sin\left(\frac{\pi}{2n}\right)\left\{\frac{\sin\left(\frac{n\psi}{2}\right)}{\sin\left(\frac{\psi}{2}\right)}\right\}\cos(\theta) \qquad (1)$$

, where $\psi = 2\pi\left[S_\lambda(1-\cos\theta)+\left(\frac{1}{2n}\right)\right]$

In Eq. 1, 'n' represents the number of turns in the helical antenna design, and 'ψ' contains the dimensional information about the array of point sources. Since the turns of the helix in the antenna are 'S_λ' turns apart, the spacing between the turns relative to λ is inserted into the program as S_λ. The $\cos(\theta)$ at Eq. 1 represents the pattern for a single turn loop antenna, which is multiplied by the Hansen-Woodyard array factor. This loop replaces each turn of the helix coil in the helical antenna approximation. This total equation now represents a single helical antenna with dimensions normalized to λ, and with 'n' turns. Since the array factors here are normalized to λ, they are frequency independent.

This helical antenna array factor is then multiplied by the simple 'MxN' element planar array factor for an array of point sources [12]:

$$AF_n = \left\{\frac{1}{M}\frac{\sin\left(\frac{M}{2}\psi_x\right)}{\sin\left(\frac{\psi_x}{2}\right)}\right\}\left\{\frac{1}{N}\frac{\sin\left(\frac{N}{2}\psi_y\right)}{\sin\left(\frac{\psi_y}{2}\right)}\right\} \qquad (2)$$

, where $\psi_x = kd_x\sin\theta\cos\phi+\beta_x$, $\psi_y = kd_y\sin\theta\sin\phi+\beta_y$

In Eq. 2, AF_n represents the normalized array factor for a planar array of M (x direction) by N (y direction) elements. We can simulate a single antenna by setting M and N equal to 1 in the Matlab simulation. Or, by setting M equal to 3 and N equal to 1, we can simulate the 3-element linear array of helical antennas which lies on a horizontal (along x-axis) plane. This would simulate the actual arrangement of helical antennas which we have made in the lab. Additionally, ψ_x and ψ_y represent the array parameters and the angular displacement vectors for solving the pattern vs. angle. $\beta_{x/y}$ represents the phase displacement between elements in the array in either the x or the y direction. This β_x would be used to adjust the phase inputs to simulate beam steering. These two array factors are simply multiplied together in Matlab and plotted vs. θ. To verify the measured antenna patterns, we first compared the measured pattern of a single helical antenna to that of the simulation program. From this comparison, we can see that the main lobe and first side lobe (FSL) locations match up very well with the simulated results. The expected and measured HPBW are also in very good agreement, as the simulated HPBW is 44.5° and the measured is 45°, as shown in Fig. 3.

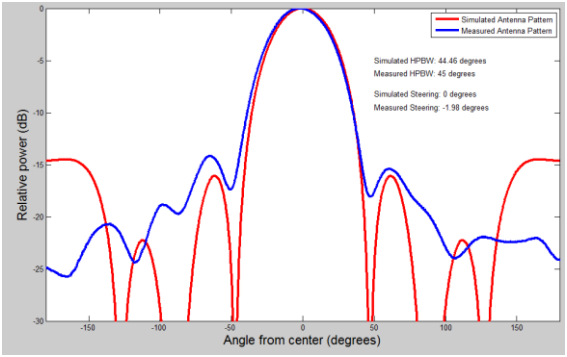

Fig. 3 Measured (blue) vs. simulated (red) radiation patterns for a single 8-turn AMHA

Additionally, the simulation results were compared with the measured radiation pattern of the un-steered (0^o) 3-element linear array of custom axial-mode helical antennas (AMHAs) in Fig. 4 [9]. The HPBW of the simulated and measured patterns are 16.7^o and 17.1^o respectively. Also, it can be seen that the side lobe locations are also in general agreement between the two patterns.

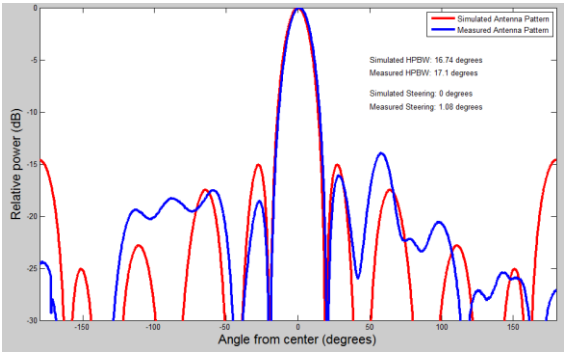

Fig. 4 Measured (blue) vs. simulated (red) radiation patterns for an un-steered 3-element array of AMHA's.

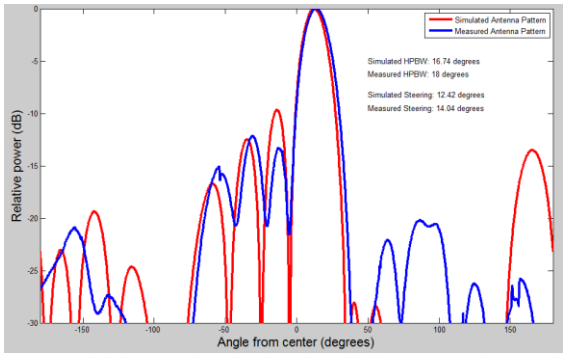

Fig. 5 Measured (blue) vs. simulated (red) radiation patterns for a 3-element array of AMHA with 90^o inter-element phase shift.

It is also important to verify that the beam steering angles we measure are in agreement with the simulation results. This helps us to make sure that there are no serious errors in the helical array design. Fig. 5 shows the simulated and measured radiation patterns for a 3-element array of AMHA's with an inter-element phase shift of 90^o in excitation signals. The physical input phase shift of the measured array is controlled by the PDM's. The non-idealities and imperfections in the physical antennas become more evident at larger steering angles, as can be seen by the slightly larger HPBW difference between the two patterns (16.7^o vs. 18^o), and the expected steering angle (12.4^o) vs. the measured steering angle (14^o). However, it is still very evident that the measured helical antenna array very well matched to the simulated expectations.

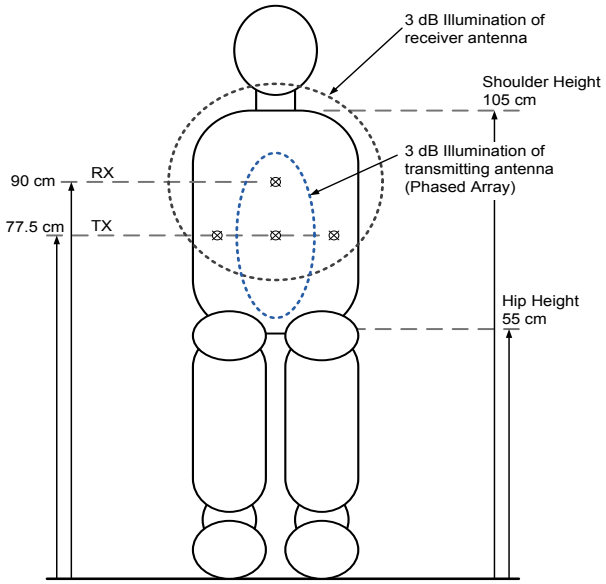

Fig. 6 Drawing of a human subject with antenna locations and 3dB beam spot locations for both the Rx and Tx phased array antennas.

III. Measured Data of Phased Array NCVS Sensor

Fig. 6 shows a drawing of a human subject with antenna locations and 3dB beam spot locations for both the Rx and Tx phased array antennas for NCVS measurement. The data shown in this section is of 15 readings of 2 minutes each, for each steering angle. This gives a total of 105 readings for the statistical measurements. For each steering angle, there are 45,000 samples of data for the analysis, which is the same number of samples used in our studies published at [8,9] for each situational difference. The data are sampled per condition at a processing rate of 25 Hz. The measured data of phased array NCVS sensor at 50, 75 and 100 cm from the subject with 7 different beam-steering conditions are provided below on student volunteers but only the 50 cm data are presented here. As the beam is steered, the Tx illumination will move away from the center of the subject (i.e., 0^o) toward the right (e.g., $+3.6^o$) or the left (e.g., -4.6^o) of the subject. Moreover, respiration rate was also measured during these experiments with an excellent ±1 breaths/minute accuracy over 95% of the time (data not shown), as the error of heart rate is higher compared to the respiration rate, due to its significantly smaller displacement. In this work, therefore, the heart rate data were used to assess system performance with different antennas setting since it is orders of magnitude smaller than the respiration signal and presents the largest challenges for robust continuous NCVS monitoring.

The measured NCVS data at 50cm away from the subject is shown in Figs. 7 and in Table 1, where Fig. 7 shows the comparison of the measured NCVS data vs. measured by the reference piezoelectric sensor taken at different Tx beam steering angles inside the anechoic chamber (in box plots). We also show the statistical analysis in Table 1 with the inter-quartile-range (IQR) and the standard deviation (STDEV) listed. It can be seen from the statistical data here, that the accuracy is rather good and is not a particularly strong function vs. the steering angle. Also, the IQR is tight, less than 0.75 BPM for all steering cases measured at 50cm. From the data, it can be seen that when the illuminating beam is steered slightly to the left or to the right of the center of the subject, the best heart rate accuracies are achieved. We speculate that the accuracy increase where the steered beam a few degrees away from the center of the monitored subject is likely caused by the relatively smaller movement of the sternum during breathing than the pectoral areas, and/or the effects of differing tissues type on the transmission and reflection of electromagnetic radiation through the body. The best case is obtained by the beam is slightly to the left (at -4.6^o), and achieved real-time heart rate error with +/- 1 beat-per-minute (BPM) 86.5% of the time, and within +/- 5 BPM 93.8% of the time during the continuous monitoring.

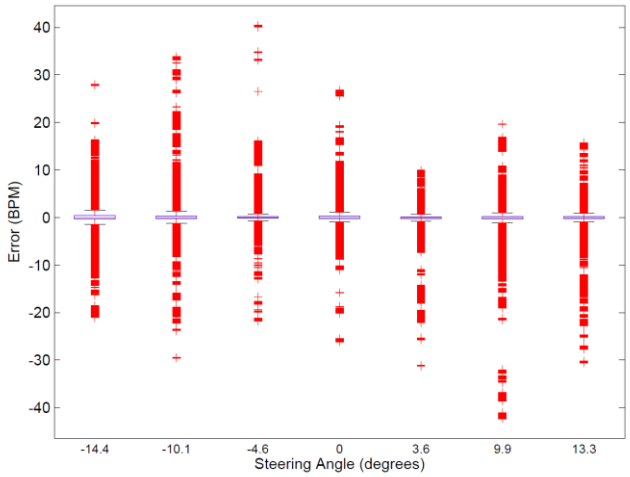

Fig. 7 Comparison of the measured data of our NCVS sensor vs. the Tx beam steering angle for data taken inside the anechoic chamber at 1 meter (in box plots)

Table I. Tabulation of the preliminary NCVS performance with helical phased array at 1 meter taken inside the anechoic chamber

	-14.4^o	*-10.1^o*	*-4.6^o*	*0^o*	*3.6^o*	*9.9^o*	*13.3^o*
1 BPM (%)	70.8	75.0	86.5	76.3	84.3	78.2	84.1
2 BPM (%)	77.3	79.8	89.5	80.3	86.9	82.5	86.9
5 BPM (%)	85.7	85.6	93.8	86.9	91.0	87.6	91.1
IQR (BPM)	0.74	0.63	0.37	0.49	0.37	0.53	0.43
STDEV (BPM)	4.14	5.88	3.44	3.67	3.86	5.52	3.83

IV. Conclusion

We have presented a 1st systematic study on phased array Doppler-based NCVS sensing results performed in a clutter-free anechoic chamber. Impressive vital signs accuracy has been achieved in real-time NCVS monitoring with a large number of data using our custom AHMA array. As brand new data has been collected and understood, we are making important strides for enabling reliable, continuous and ubiquitous NCVS monitoring in the near future. More work is on-going to study the effects of clutters on the NCVS sensing accuracy to prepare for a small-scale clinical trial after the IRB approval.

Acknowledgment

We are indebted to Prof. T. Trost at Texas Tech University for all his guidance on antenna measurement.

References

[1] D. J. Limmer, M. F. O'Keefe, H.T. Grant, B. Murray, D. Bergeron and E.T. Dickinson, *Emergency Care*, Eleventh Edition, Prentice Hall, N.J., (2008)

[2] C.G. Caro and J.A. Bloice, "Contactless apnea detector based on radar", Lancet; vol 2, no.7731, pp 959-961, Oct. (1971)

[3] C.I. Franks, B.H. Brown and D.M. Johnston, "Contactless respiration monitoring of infants", *Med. Biol. Eng. 14(3):306-312,* May (1976)

[4] C.I. Franks, J. B. Watson, B. H. Brown and E. F. Foster, "Respiratory patterns and risk of sudden unexpected death in infancy", *Arch. Dis. Child*; 55(8):595-604, (1980)

[5] J.C. Lin, "Microwave sensing of physiological movement and volume change: A review", Bioelectromagnetics, 13, pp. 557-565, Dec. (1992)

[6] A.D. Droitcour, "Non-contact measurement of heart and respiration rates with a singlechip microwave Doppler radar", *Doctoral Thesis, Stanford University, CA (*2006)

[7] B.K. Park; S. Yamada, O. Boric-Lubecke and V. Lubecke, "Single-channel receiver limitations in Doppler radar measurements of periodic motion", *IEEE Radio Wireless Symp.,* pp. 99- 102, 17-19 Jan. (2006)

[8] V. Das, A. Boothby, R. Hwang, T. Nguyen, J. Lopez, D.Y.C. Lie, "Antenna evaluation of a non-contact vital signs sensor for continuous heart and respiration rate monitoring," *IEEE Topical Conference on Biomedical Wireless Technologies, Networks, and Sensing Systems (BioWireleSS)*, pp.13-16, 15-18 Jan. (2012)

[9] A. Boothby, R. Hwang, V. Das, J. Lopez, D.Y.C. Lie, "Design of Axial-mode Helical Antennas for Doppler-based continuous non-contact vital signs monitoring sensors", *IEEE Radio and Wireless Symposium (RWS)*, pp.87-90, 15-18 Jan. (2012)

[10] B.K. Park, O. Boric-Lubecke and V. Lubecke, "Arctangent Demodulation with DC Offset Compensation in Quadrature Doppler radar Receiver Systems", *IEEE Trans. Microw. Theory Tech., 55, 5*, pp.1073-1079, (2007)

[11] R. Ichapurapu, S. Jain, M.U. Kakade, D.Y.C. Lie, and R.E. Banister, "A 2.4GHz non-contact biosensor system for continuous vital-signs monitoring on a single PCB", Proc. IEEE 8th Int'l Conf. on ASIC (ASICON09), pp. 925-928, Changsha, China, 20-23 Oct. (2009)

[12] C. A. Balanis, *Antenna Theory*, Second Edition, John Wiley & Sons, NY, (1997)

[13] J. D. Kraus, *Antennas*, Second Edition, McGraw-Hill, N.Y., (1988)